Cluster tool for in situ processing and comprehensive characterization of thin films at high temperatures

Originally published:

May 2018

Analytical Chemistry 90(2018), 7837-7842

DOI: https://doi.org/10.1021/acs.analchem.8b00923

Technical Note

Cluster tool for *in situ* processing and comprehensive characterization of thin films at high temperatures

Robert Wenisch, Frank Lungwitz, Daniel Hanf, Rene Heller, Jens Zscharschuch, René Hübner, Johannes von Borany, Gintautas Abrasonis, Sibylle Gemming, Ramon Escobar-Galindo, and Matthias Krause

Anal. Chem., **Just Accepted Manuscript** • DOI: 10.1021/acs.analchem.8b00923 • Publication Date (Web): 31 May 2018

Cluster tool for *in situ* processing and comprehensive characterization of thin films at high temperatures

Robert Wenisch,[†] Frank Lungwitz,[†] Daniel Hanf,[†] René Heller,[†] Jens Zscharschuch,[†] René Hübner,[†] Johannes von Borany,[†] Gintautas Abrasonis,[†] Sibylle Gemming,[†,‡] Ramon Escobar-Galindo,[‡] Matthias Krause[†,*]

[†]Helmholtz-Zentrum Dresden-Rossendorf, Bautzner Landstr. 400, 01328 Dresden, Germany, [‡]Technische Universität Chemnitz, Reichenhainer Straße 70, 09126 Chemnitz, Germany, [‡] Departamento de Ciencia de los Materiales e Ingeniería Metalúrgica y Química Inorgánica, IMEYMAT, Universidad de Cádiz, 11510 Puerto Real, Spain

*matthias.krause@hzdr.de, +49 351 260 3578

ABSTRACT: A new cluster tool for *in situ* real-time processing and depth-resolved compositional, structural and optical characterization of thin films at temperatures from -100 to 800 °C is described. The implemented techniques comprise magnetron sputtering, ion irradiation, Rutherford backscattering spectrometry, Raman spectroscopy and spectroscopic ellipsometry. The capability of the cluster tool is demonstrated for a layer stack MgO/ amorphous Si (~60 nm)/ Ag (~30 nm), deposited at room temperature and crystallized with partial layer exchange by heating up to 650°C. Its initial and final composition, stacking order and structure were monitored *in situ* in real time and a reaction progress was defined as a function of time and temperature.

High-temperature (high-T) materials and applications have gained increasing scientific interest and technological importance for about 20 years. They are often related to energy conversion and so-called new energy materials. Currently studied high-T applications are solid-oxide fuel cells,[1,2] concentrated solar power (CSP) generation,[3,4] exhaust gas heat recovery by thermoelectricity,[5,6] and high-T sensors.[7,8] Required working temperatures for these applications are in the range of 600 to 1000 °C. Relevant material systems are often thin films of sub-nm to 1 µm thickness that are comprised of sophistically designed multilayers for achieving the full functionality. Intra- and interlayer phase transitions, defect generation and annealing, degradation processes, such as element redistribution and interface mixing, as well as material exchange with the environment can have substantial effects on their structure, properties and functionality. To ensure thin film's functionality under high-T conditions, new concepts for analysis and process monitoring are necessary. Suitable processing abilities are required, and composition, structure as well as functionality have to be monitored *in situ* in real time.

Cluster tool setups integrate a number of dedicated chambers into a single experimental system and enable multistep experiments at controlled conditions. This concept combines fast sample transfer with moderate lab space requirements and prevents mutual interference of the different experimental techniques. For thin film technology, high vacuum (HV) or even ultra-high vacuum (UHV) conditions are required. In this technical note, a new cluster tool comprising magnetron sputtering (MS), ion irradiation, Rutherford backscattering spectrometry (RBS), Raman spectroscopy and spectroscopic ellipsometry (SE) is described.[9] MS is a scalable, clean and waste-free industry-relevant physical vapor deposition technique. RBS yields depth-resolved atomic concentrations for elements with $Z \geq 6$. Raman spectroscopy offers outstanding structure sensitivity and monolayer detection. Ellipsometry provides nm-precise thickness information for single layers, multilayers and mixtures, and in addition, the determination of the optical constants of the sample's components. These techniques are appropriate for thin film technology and distinguish this setup from existing cluster tools, which mainly rely on X-Ray- and electron-based detection techniques, whose information depth and depth resolution are limited.[10,11,12,13,14]

The capability of the new cluster tool is demonstrated for the model system MgO/ amorphous silicon (a-Si) (~60 nm)/ Ag (~30 nm), which was deposited at room temperature (RT) and heated up to 650 °C. Initial and final composition, stacking order and structure of the involved materials were analyzed *in situ* in real time. The reaction progress was monitored as function of time and temperature by three complementary methods. Metal-induced crystallization (MIC) is identified as responsible reaction mechanism.

EXPERIMENTAL SECTION

The cluster tool is installed as end station at an ion beamline of the Ion Beam Center (IBC) at the Helmholtz-Zentrum Dresden-Rossendorf (HZDR).[15] Four chambers

are connected to the central transfer chamber (Prevac) (Figure 1). Temperatures from -100 to 1000 °C can be applied to the sample in all chambers, and *in situ* monitoring is possible from -100 to 800 °C. The setup enables the reproducible sample transfer from one chamber to another within less than 30 s. The maximum sample size is 25 mm in diameter.

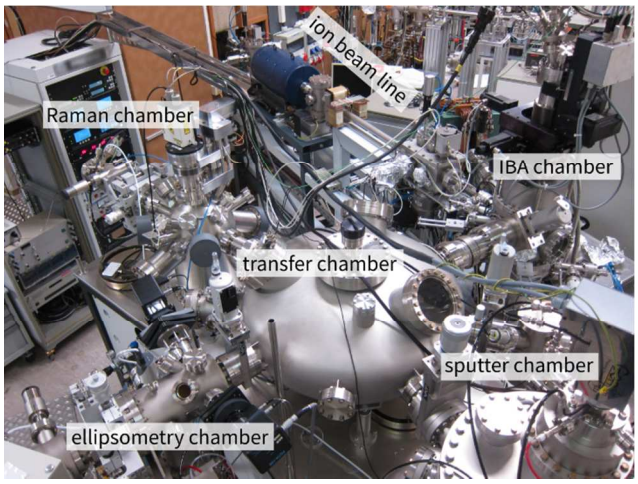

Figure 1: Cluster tool connected to ion beamline no. 9 of the 6 MV tandem accelerator of the IBC. The setup has a size of about 5 m × 5 m.

The sputter chamber for sample pre-treatment, deposition and patterning is equipped with two direct current (DC) magnetrons (Thin Film Consulting ION'X-2" UHV) and an ECR ion source (Tectra Gen II). The magnetrons are designed for a working pressure of 0.1 to 10 Pa of Ar for operation at an electrical power of up to 400 W. They are bordered by chimneys to prevent excessive contamination of the chamber walls, and are mounted in a 180° geometry, thus excluding co-sputtering. The magnetron to sample distance is approximately 10 cm. The ECR ion source is mounted in a 90° geometry to the magnetrons and enables sputter cleaning and ion-induced pre-patterning of substrates. It can deliver ion beam currents of up to 60 mA at ion energies of 0.2 to 2.5 keV. Its maximum working pressure is 0.1 Pa in the vacuum chamber, preventing simultaneous operation of the magnetrons and the ion source.

The ion beam analysis (IBA) chamber (Figure 2) is connected to a 6 MV tandem accelerator, which provides a wide range of ion species. For RBS measurements, He^+ ions of 2 MeV are commonly used. An ion current of approx. 20 nA provides a good signal to noise ratio and prevents beam-induced sample damage and unintentional heating. A multi-stage setup with a double-magnetic quadrupole, two crossed magnetic dipoles, 3 scintillators (Al_2O_3), 3 Faraday cups and a beam chopper system is used for beam alignment, fine tuning and monitoring. The sample holder is positioned onto a 5-axis manipulator, which bears also one of the scintillators and one of the Faraday cups (Figure 2). A beam spot diameter of < 1 mm is achieved on the sample, and the positioning reproducibility is 100 µm. The backscattered ions are detected at a backscattering angle of 155° by a silicon detector (SiD) covered by 100 nm Al to reduce its sensitivity to near-infrared and visible light. Nevertheless, detector saturation by thermal radiation limits the accessible temperature for *in situ* RBS to 800 °C. The time resolution is 30 s for qualitative analysis and 1 min if quantitative evaluation is desired. The SiD energy resolution is about 18 keV. The depth resolution is of the order of 15 nm for near-surface regions, where energy straggling is negligible.

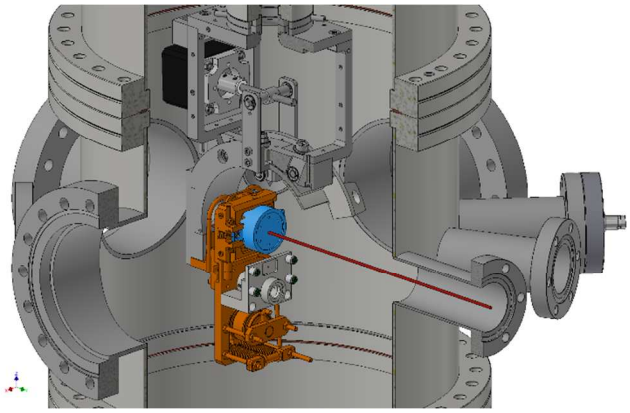

Figure 2: Drawing of the IBA chamber. The ion beam axis is indicated as a red line, the sample holder is depicted in blue color. The Faraday cup for measuring the beam current at the sample and a quartz scintillator for beam alignment are mounted directly below the sample holder (light gray color).

The Raman chamber is optimized for maximum light-throughput and high sensitivity. Glass fiber optics connect exciting lasers, remote measurement head, Raman chamber and spectrometer. A diode-pumped solid-state laser and a frequency-doubled Nd:YAG laser with wavelengths of 473 and 532 nm, respectively, are used for excitation. The remote head and a purpose-built macro extension optics (Horiba Jobin-Yvon) with a numerical aperture of 0.22 and a focus length of 80 mm are used for focusing and collection of light. The lateral and depth resolution of the collection optics are 60 µm and approximately 270 µm, respectively. The macro extension optics is mounted outside the UHV, leaving a small air slit between it and the transparent window of the Raman chamber. A motorized linear translation stage is used for defined focusing onto the sample surface. Sample monitoring is managed by video cameras. The 180° backscattered Raman light is first guided through the Rayleigh and interference filters of the remote head and subsequently dispersed by an iHR 550 spectrograph (Horiba Jobin-Yvon) equipped with changeable 300/ mm, 600/ mm and or 1800/ mm holographic gratings. For the detection of the Raman light a liquid nitrogen-cooled CCD detector with a back-illuminated deep-depletion chip is used. Its quantum efficiency exceeds 90 % in the entire spectral range from 400 to 800 nm. CCD oversaturation with thermal photons limits *in situ* Raman experiments to 800 °C.

The ellipsometry chamber is equipped with a M2000V ellipsometer (J.A. Woollam Co.). The exciting light is emitted by a Quartz-Tungsten-Halogen lamp and covers an energy range from 1.24 to 3.31 eV, corresponding to a wavelength range of 1000 to 375 nm. The incidence angle is 70.5° with respect to the sample normal. Opposing the light source, the CCD detector is mounted under an identical angle. A rotating compensator enables simultaneous measurements of all wavelengths and therefore data acquisition in few seconds. The optical detection limits the accessible temperature range to 800 °C. Among the three analytical techniques used, the SE has the best time and depth resolution. A special feature of the ellipsometry chamber is a gas inlet system enabling studies of optical properties in oxygen, nitrogen and argon as well as in mixtures of them. The most relevant specifications of the techniques implemented in the cluster tool are summarized in Table 1.

Table 1: Performance parameters of the techniques implemented in the cluster tool. (n.a.: not applicable)

Technique	Maximum temperature (°C)	Time resolution (s)	Depth resolution	Lateral resolution
DC - MS	1000	n.a.	n.a.	n.a.
RBS	800	30	15 nm	1 mm
Raman	800	30	270 µm	60 µm
SE	800	5	1 nm	2 mm × 10 mm

To show the capabilities of the cluster tool, three samples of the model system MgO (bulk)/ a-Si (~60 nm)/ Ag (~30 nm) were deposited by DC-MS at room temperature (RT) at ≈1 Pa with deposition rates (powers) of 2.3 nm/ min (40 W) for Si and 8.5 nm/ min (10 W) for Ag and subsequently heated in HV in independent RBS, Raman spectroscopy and SE experiments with a constant ramp rate of 0.3 K/ s between 100 and 650 °C. The maximum temperature was kept for an hour after which the samples were cooled with a rate of -0.3 K/ s. The samples were kept in vacuum (10^{-5} Pa for RBS and SE, 10^{-7} Pa for Raman) throughout the experiments except for a short duration (< 30 min) in air between the deposition and the heating step in order to change the sample holder. In this way, always the same sample holder is used for depositions, without exposing it to high temperatures. This procedure ensures the best possible reproducibility of the deposition process and thus, of sample composition. This change may however only be applied, if the studied materials are inert in air. Since the RBS spectrum of the as-deposited layer stack shows no intensity bump at the high-energy edge of the substrate's oxygen signal, this condition is fulfilled in this study.

RESULTS AND DISCUSSION

The RBS spectrum of the virgin sample shows the signals of Mg and O atoms in the substrate as two plateau-like features (Figure 3a)). The distinct peaks at higher backscattering energy are attributed to the Ag and Si layer (Figure 3 a)). A quantitative fitting procedure using SIMNRA[16] reveals areal densities of 1.6×10^{17} atoms cm^{-2} and 2.8×10^{17} atoms cm^{-2} for Ag and Si, respectively. Following the initial characterization, the thermal treatment was started and monitored *in situ* as a function of time and temperature (Figure 3 b)). Upon reaching a temperature of 580 °C, the Ag peak broadened and shifted to a lower backscattering energy by about 0.02 MeV. Thus, the Ag depth distribution was broadened and its center of gravity moved towards the substrate. Simultaneously, the Si peak was broadened and split into two sub-peaks at first glance, indicating the re-distribution of the whole Si layer, a part of it having moved towards the surface. The Mg and O edges were unchanged in energy but slightly broadened (Figure 3 c)), i.e. the total stopping power of the Si/Ag bilayer did not change. The latter observation points to conserved total atomic concentrations of Ag and Si within the layer stack.

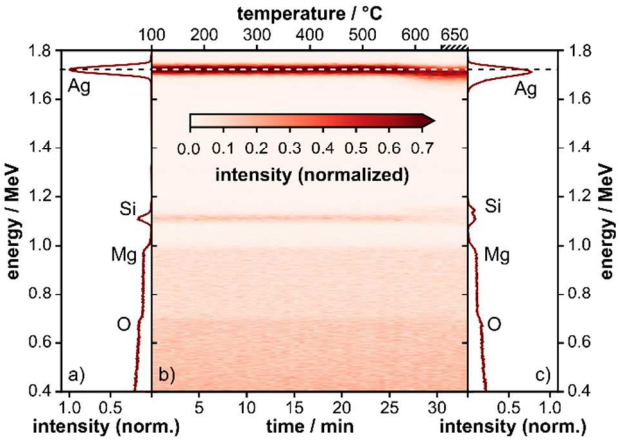

Figure 3: *In situ* RBS analysis of the MgO/ a-Si/ Ag stack. a) RBS spectrum at RT of the as-deposited stack, b) RBS mapping from 100 to 650 °C, c) RBS spectrum at RT of the final layer stack after the heating experiment. The temperature was held constant upon reaching 650 °C as indicated by the hatched stripe of the temperature axis.

Importantly, the processes occurred at high temperatures and not after re-cooling. Neither by continued heating to 650 °C, a 1 h hold at this temperature nor by re-cooling to RT, further changes of the RBS spectra occurred. Fitting the RBS data by SIMNRA[16] turned out to be complicated, presumably due to the lateral and in-depth inhomogeneity generated in the sample during the *in situ* annealing.

The Raman spectrum of the initial stack shows no signal from RT to about 520 °C, since the Ag top layer is Raman-inactive and optically non-transparent (Figure 4a)). Accordingly, any Raman signal would only appear after the Si/ Ag stacking order change had started.

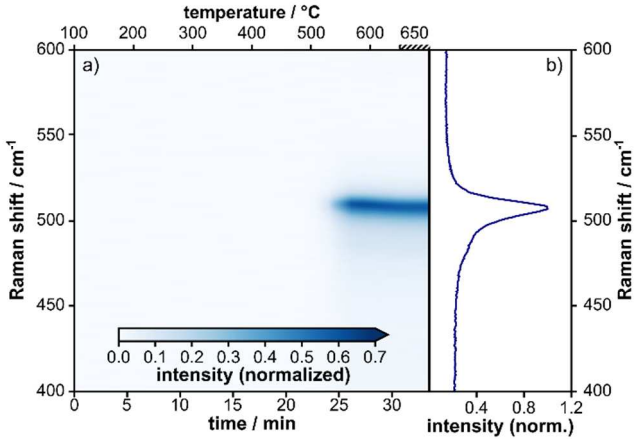

Figure 4: *In situ* Raman analysis of the MgO/ a-Si/ Ag stack. a) Raman mapping from RT to 650°C. b) Raman spectrum of the final layer stack taken at 650°C. The hatched stripe in the temperature axis has the same meaning as in fig. 3.

At about 520 °C, the Γ-point vibration of crystalline silicon (c-Si) appeared at around 515 cm^{-1} as dominant spectral signature. It shifts to slightly lower frequencies with further increasing temperature (Figure 4a)).[17,18] Moreover, the asymmetric broadening of the c-Si line to lower Raman shifts (Figure 4a, 4b)), indicates minor amounts of defective silicon (def-Si), i.e. either wurtzite-type[19,20] or near-surface Si[21,22], and of non-crystallized a-Si[23] in the final layer stack. The line shape analysis of the final stack's RT *in situ* Raman spectrum gave Raman shifts of 522 cm^{-1} for c-Si, 500 cm^{-1} for def-Si and 480 and 440 cm^{-1} for the a-Si lines. Their relative integral intensities were 80 %, 5 %, 9 % and 6 %, respectively, obtained by fitting the spectrum with a BWF line for c-Si and Gaussians for def-Si and a-Si. The crystalline Si volume fraction ρ_c was estimated from the integral Raman intensities by equation (1), wherein the intensity of the 440 cm^{-1} line is not included:[24]

$$\rho_c = \frac{I_{c-Si} + I_{def-Si}}{I_{c-Si} + I_{def-Si} + yI_{a-Si}} \qquad (1).$$

The crystallite size dependent integrated Raman cross sections, $y = \Sigma_{c\text{-}Si}/\Sigma_{a\text{-}Si}$, determines the Raman line shape of the crystalline Si.[24,25] Since a BWF shape was found to fit the c-Si profile best, the minimum crystallite size L is $L \geq 15$ nm and thus, the minimum y-value is $y = 0.65$.[24] With equation (1), the c-Si volume fraction is estimated to be ≥ 90 %.

As third characterization technique, *in situ* SE of the model system was measured continuously as a function of temperature. 100 acquisitions of both, the amplitude ratio ψ and the phase shift Δ were recorded every 11.5 seconds during the heating process, resulting in ~ 750 spectra for the two parameters (Figure 5).

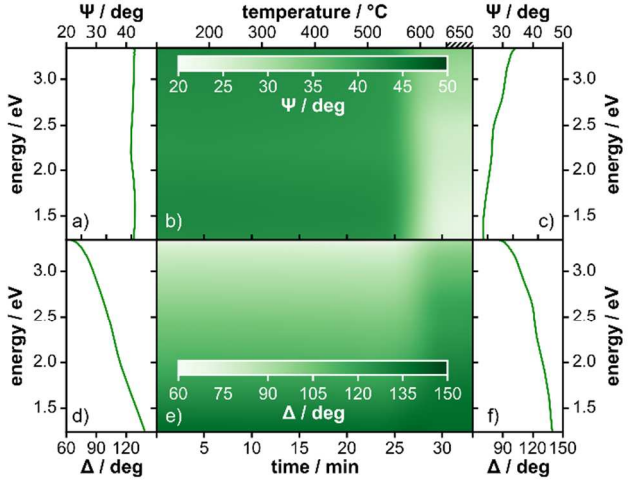

Figure 5: *In situ* spectroscopic ellipsometry of the MgO/ a-Si/ Ag stack as a function of temperature. a), d) Measured Ψ and Δ of the virgin sample at RT. b), e) *in situ* mapping of Ψ and Δ from 120 to 650 °C. c), f) Ψ and Δ of the final sample measured at 650 °C. The hatched stripe in the temperature axis has the same meaning as in fig. 3.

A distinct change in the ellipsometry parameters occurred, when the temperature of about 580 °C was reached (Figure 5b) and e)). This change is also apparent form the comparison of ψ and Δ of the as-deposited (Figure 5 a), d)) and thermally processed layer stack (Figure 5 c), f)). The SE data were analyzed with the software WVASE32 (J.A. Woollam Co.). The spectrum of the virgin sample was modelled by a three-layer system consisting of MgO substrate, a-Si and Ag by fitting reference data from WVASE32 and the literature to the measured spectra.[26,27] Layer thicknesses of 34±1 nm (Ag) and 65±3 nm (a-Si) were obtained. Combining areal densities measured by RBS and SE spectra, mass densities of 2.0 g cm^{-3} and 8.5 g cm^{-3} for the virgin a-Si and Ag layer, respectively, are obtained in agreement with literature data of sputtered a-Si and Ag thin films.[28-31] By supplementary transmission electron microscopy (TEM), an a-Si thickness of 63 nm was found in full agreement with the SE. Unfortunately, the Ag thickness could not be cross-checked by TEM because the Ag layer got modified during lamella preparation.

The final SE spectrum of the heating experiment could not be described by a model stack of homogenous layers. Its simulation required assuming a stack with effective medium approximation (EMA) layers[32-34] containing different volume fractions of Ag and c-Si. The obtained fit model with a total thickness of 105 nm comprised 3 main, Bruggeman-type EMA layers consisting of Ag and c-Si, a 5 nm thick surface roughness layer and a 5 nm thick EMA bottom layer of c-Si and MgO. The thicknesses of three main EMA layers were 19 nm (top), 27 nm (middle) and 49 nm (bottom), and their atomic compositions were 62 at.% c-Si/ 38 at.% Ag (top), 46 at.% c-Si/ 54 at.% Ag (middle) and 83 at.% c-Si/ 17 at.% Ag (bottom), respectively. This model reproduced qualitatively the shape and major features of the experimental data. It accounts for the partial up-shift and the double-peak structure of the

Si-RBS-signal, its general broadening and for the down-shifted and broadened Ag-RBS-peak. It is also consistent with the dominance of c-Si within the total Si volume fraction obtained by Raman spectroscopy. Nevertheless it has to be noted that the obtained specific numbers have to be taken with care because of the large number of unknowns for fitting of SE data by EMA models.

In situ real time RBS, Raman spectroscopy as well as SE showed consistently a structural transformation of an initial MgO/ a-Si (~60 nm)/ Ag (~30 nm) model stack in the temperature range from 530 to 580 °C, which resulted in the almost complete crystallization of a-Si and a partial layer exchange. In the final layer stack an Ag-rich layer was sandwiched by two c-Si-rich layers. From the mechanistic point of view, the reaction is attributed to a MIC[35,36] and not to a dissolution-precipitation process, since it occurred at high temperatures and not during re-cooling. This process can be further characterized in terms of a reaction progress, defined for all three analytical methods (Figure 6). For Raman spectra, this was done straightforwardly by assigning the reaction progress to the intensity of the c-Si line, normalized to its final value. For SE, the reaction progress was assigned to the normalized average spectral values. The RBS spectra were decomposed into a linear combination of initial and final spectrum, and the coefficient of the final one was assigned as reaction progress. According to figure 6, the total transition time was of the order of 4 min. The precise values for the transition duration from steepest slopes of the reaction progress are (4.0±0.5) min for Raman spectroscopy, (3.7±0.3) min for Rutherford backscattering spectrometry and (4.1±0.3) min for spectroscopic ellipsometry. The transition temperature, defined as the temperature yielding the largest value of the first derivative of the reaction progress functions, was in the range of 540 to 580°C. The observed variation of the transition temperature is much smaller than that reported in the literature for this system, which covered a range from 385 °C to 540 °C.[37,38] The slightly lower value obtained by Raman spectroscopy can be tentatively attributed to a laser-induced photo or heating effect.

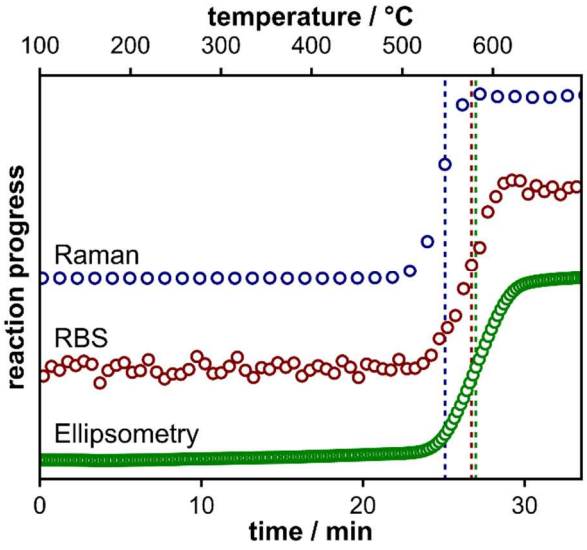

Figure 6: Reaction progress as function of time and temperature measured by Raman spectroscopy, RBS and SE. The critical temperature corresponds to the transformation temperature and is indicated by vertical dashed lines.

SUMMARY AND CONCLUSION

A new cluster tool was described. Its capabilities were demonstrated for the real-time *in situ* analysis of structural changes of the model system MgO/ a-Si (~60 nm)/ Ag (~30 nm) as a function of temperature under high vacuum conditions. The complementary analytical techniques of the setup, RBS, Raman spectroscopy and spectroscopic ellipsometry, allow the determination of thin film properties not accessible by one technique alone. This holds independently on the materials structure, i.e. whether they are crystalline or amorphous. In this sense, the new cluster tool is a unique new setup for *in situ* processing and comprehensive characterization of thin films in the temperature range from -100 to 800 °C.

AUTHOR INFORMATION

Corresponding Author

*Dr. Matthias Krause, Helmholtz-Zentrum Dresden-Rossendorf, Bautzner Landstr. 400, 01328 Dresden, Germany, matthias.krause@hzdr.de

Present Addresses

†R. Wenisch, present address: PVcomB, Helmholtz-Zentrum Berlin, Schwarzschildstraße 3, Berlin, 12489, Germany.

Author Contributions

The manuscript was written through contributions of all authors. All authors have given approval to the final version of the manuscript.

Funding Sources

Funding was provided by H2020 RISE project "Framework of Innovation for Engineering of New Durable Solar Surfaces (FRIENDS^2, GA-645725)" and Initiative and Networking Funds of the president of the Helmholtz Association via the W2/W3 program (SG).

ACKNOWLEDGMENT

Support of the Ion Beam Center (IBC) at HZDR, its operator team and technical assistance by Angela Schneider, Annette Kunz and Romy Aniol is gratefully acknowledged.

REFERENCES

(1) Badwal, S. P. S.; Giddey, S.; Munnings, C.; Kulkarni, A. *J. Aust. Ceram. Soc.* **2014**, *50*, 23-37.
(2) Irshad, M.; Siraj, K.; Rizwan, R., et al. *Appl. Sci.* **2016**, *6*, 75-97.
(3) Weinstein, L. A.; Loomis, J.; Bhatia, B.; et al. *Chem. Rev.* **2015**, *115*, 12797.
(4) Selvakumar, N.; Barshilia, H. C. *Sol. Energy Mater. Sol. Cells* **2012**, *98*, 1-23.
(5) Fergus, J. W. *J. Eur.Ceram. Soc.* **2012**, *32*, 525-540.
(6) Backhaus-Ricoult, M.; Rustad, J.; Moore, L.; Smith, C.; Brown, J. *Appl. Phys. a-Materials Science & Processing* **2014**, *116*, 433-470.
(7) Zhang, S. J.; Yu, F. P. *J. Am. Ceram. Soc.* **2011**, *94*, 3153-3170.

(8) Fergus, J. W. *Sens. Actuators B-Chemical* **2007**, *121*, 652-663.
(9) Wenisch, R. In Situ and Ex Situ Investigations of Transition Metal-Catalyzed Crystallization of Carbon and Silicon Thin Films. Technische Universität Chemnitz, 2017.
(10) J311 UHV System with UPS/XPS/IPES. http://ee.princeton.edu/research/kahn/?q=node/7 (accessed 2017-11-30).
(11) The ORPHEUS Cluster (accessed 2017-11-23).
(12) The Nano-Spintronics-Cluster-Tool (accessed 2017-11-23).
(13) Helmholtz-Zentrum Berlin für Materialien und Energie, *JLSRF* **2016**, *2*, A67.
(14) Lips, K.; Starr, D. E.; Bar, M.; Schulze, T. F.; et al., *IEEE 40th Photovoltaic Specialist Conference (Pvsc)* **2014**, 698-700.
(15) User facilities at the Ion Beam Center. https://www.hzdr.de/db/Cms?pOid=29003&pNid=1984 (accessed 2018-02-08).
(16) Mayer, M. SIMNRA User's Guide.
(17) Hart, T. R.; Aggarwal, R. L.; Lax, B. *Phys. Rev. B* **1970**, *1*, 638.
(18) Temple, P. A.; Hathaway, C. E. *Phys. Rev. B* **1973**, *7*, 3685-3697.
(19) Kobliska, R. J.; Solin, S. A. *Phys. Rev. B* **1973**, *8*, 3799-3802.
(20) Lopez, F. J.; Hemesath, E. R.; Lauhon, L. J. *Nano Lett.* **2009**, *9*, 2774-2779.
(21) Xia, H.; He, Y. L.; Wang, L. C.; Zhang, W.; et al. *J. Appl. Phys.* **1995**, *78*, 6705-6708.
(22) Smit, C.; van Swaaij, R.; Donker, H.; Petit, A.; et al. *J. Appl. Phys.* **2003**, *94*, 3582-3588.
(23) Iqbal, Z.; Veprek, S. *J. Phys.: Condens. Matter* **1982**, *15*, 377-392.
(24) Bustarret, E.; Hachicha, M. A.; Brunel, M. *Appl. Phys. Lett.* **1988**, *52*, 1675-1677.
(25) Tsu, R.; Gonzalezhernandez, J.; Chao, S. S.; Lee, S. C.; Tanaka, K. *Appl. Phys. Lett.* **1982**, *40*, 534-535.
(26) Synowicki, R. A. *Thin Solid Films* **2004**, *455-456*, 248-255.
(27) Palik, E. D. Handbook of optical constants of solids; Elsevier, 1997.
(28) Pelaz, L.; Marques, L. A.; Barbolla, J. *J. Appl. Phys.* **2004**, *96*, 5947-5976.
(29) Pawlewicz, W. T. *J. Appl.Phys.***1978**, *49*, 5595-5601.
(30) Kizuka, T.; Nakagami, Y.; Ohata, T.; Kanazawa, I.; et al. *Philos. Mag. A* **1994**, *69*, 551-563.
(31) Kundu, S.; Hazra, S.; Banerjee, S.; Sanyal, M. K.; et al. *J. Phys. D: Appl. Phys.* **1998**, *31*, L73-L77.
(32) Fujiwara, H. *Spectroscopic ellipsometry: principles and applications*; John Wiley & sons: Chichester, 2007.
(33) Bruggeman, D. A. G. *Ann. Phys.* **1935**, *24*, 636-664.
(34) Heras, I.; Krause, M.; Abrasonis, G.; Pardo, A.; et al. *Sol. Energy Mat. Sol. Cells* **2016**, *157*, 580-590.
(35) Wang, Z.; Jeurgens, L. P. H.; Wang, J. Y.; Mittemeijer, E. J. *Adv. Eng. Mater.* **2009**, *11*, 131-135.
(36) Wang, Z; Jeurgens, L. P. H.; Mittemeijer, E. J. *Metal-Induced Crystallization*; Pan Stanford Publishing Pte. Ltd.: Singapore, 2015.
(37) Bian, B.; Yie, J.; Li, B.; Wu, Z. *J. Appl. Phys.* ***1993,*** 73, 7402-7406.
(38) Knaepen, W.; Detavernier, C.; Van Meirhaeghe, R. L.; Sweet, J. J.; Lavoie, C. *Thin Solid Films* ***2008****, 516,* 4946-4952.

For TOC only

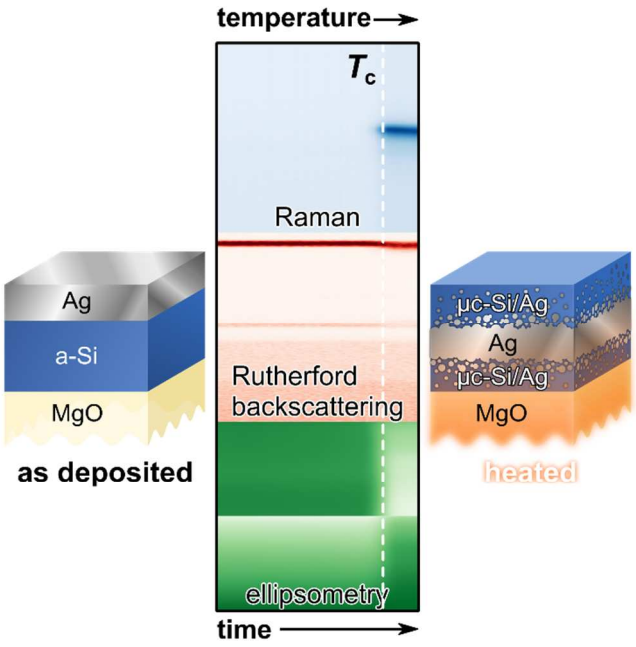
temperature
T_c
Raman
Rutherford
backscattering
ellipsometry
time
Ag
a-Si
MgO
as deposited
μc-Si/Ag
Ag
μc-Si/Ag
MgO
heated

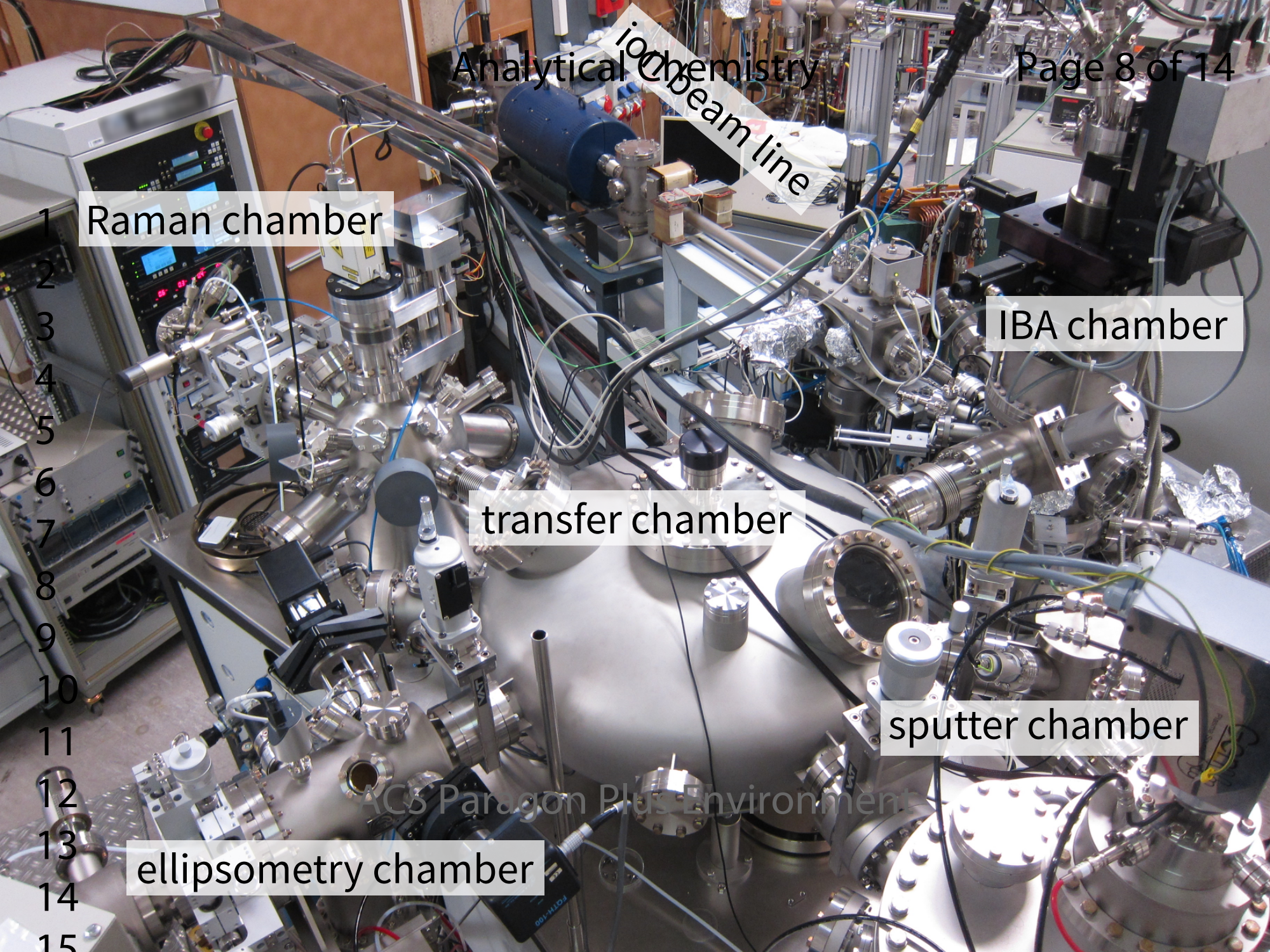

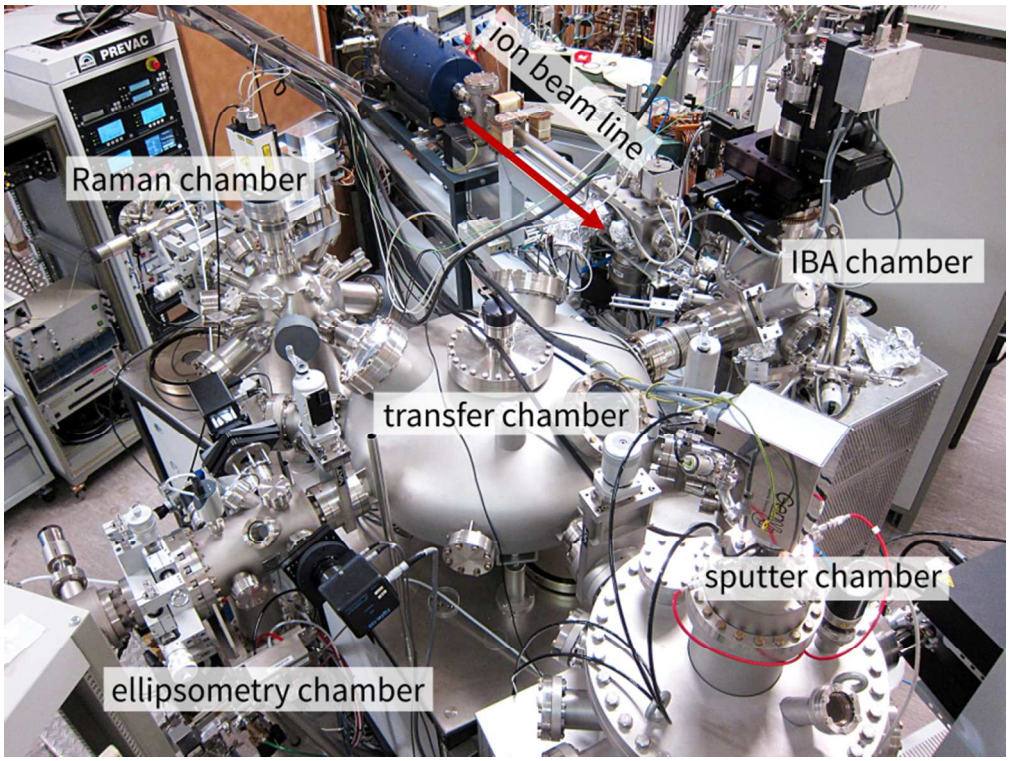

Figure 1

200x150mm (150 x 150 DPI)

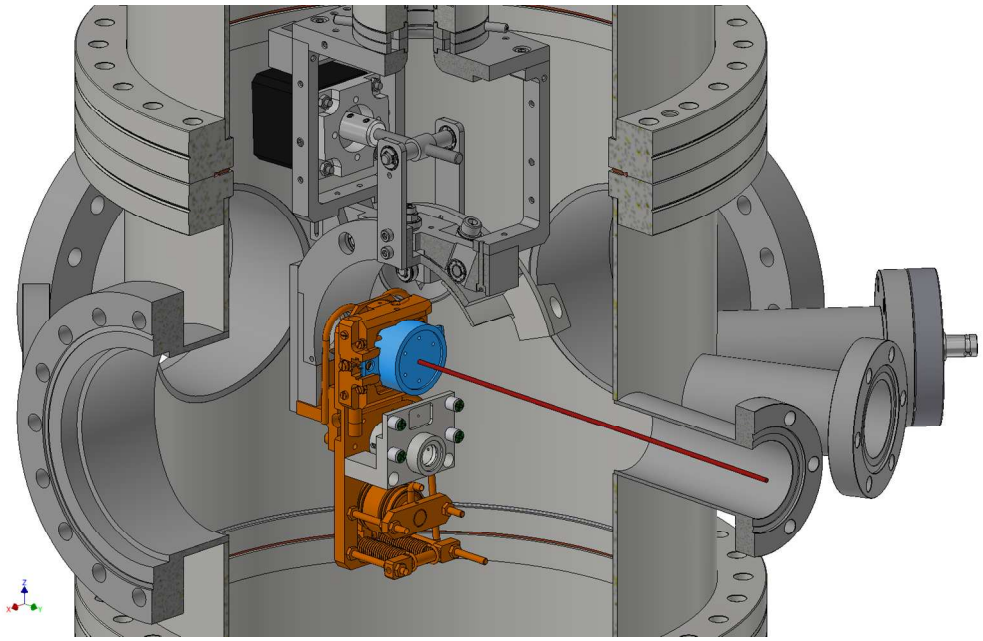

Figure 2

426x268mm (96 x 96 DPI)

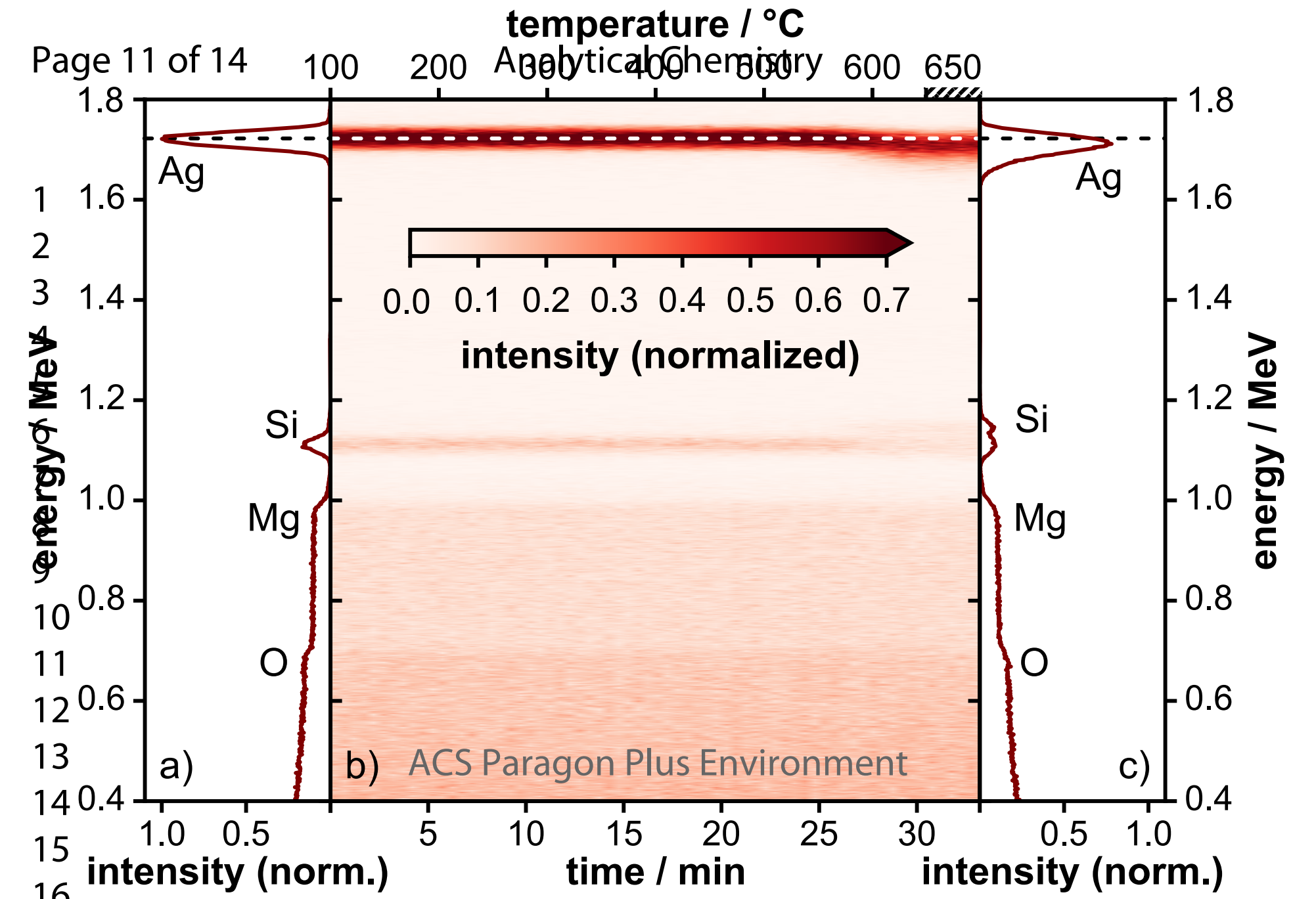
temperature / °C
100
200
300
400
500
600
650
1.8
1.6
1.4
1.2
1.0
0.8
0.6
0.4
energy / MeV
Ag
Si
Mg
O
0.0 0.1 0.2 0.3 0.4 0.5 0.6 0.7
intensity (normalized)
a)
b)
ACS Paragon Plus Environment
c)
1.0 0.5
intensity (norm.)
5 10 15 20 25 30
time / min
0.5 1.0
intensity (norm.)

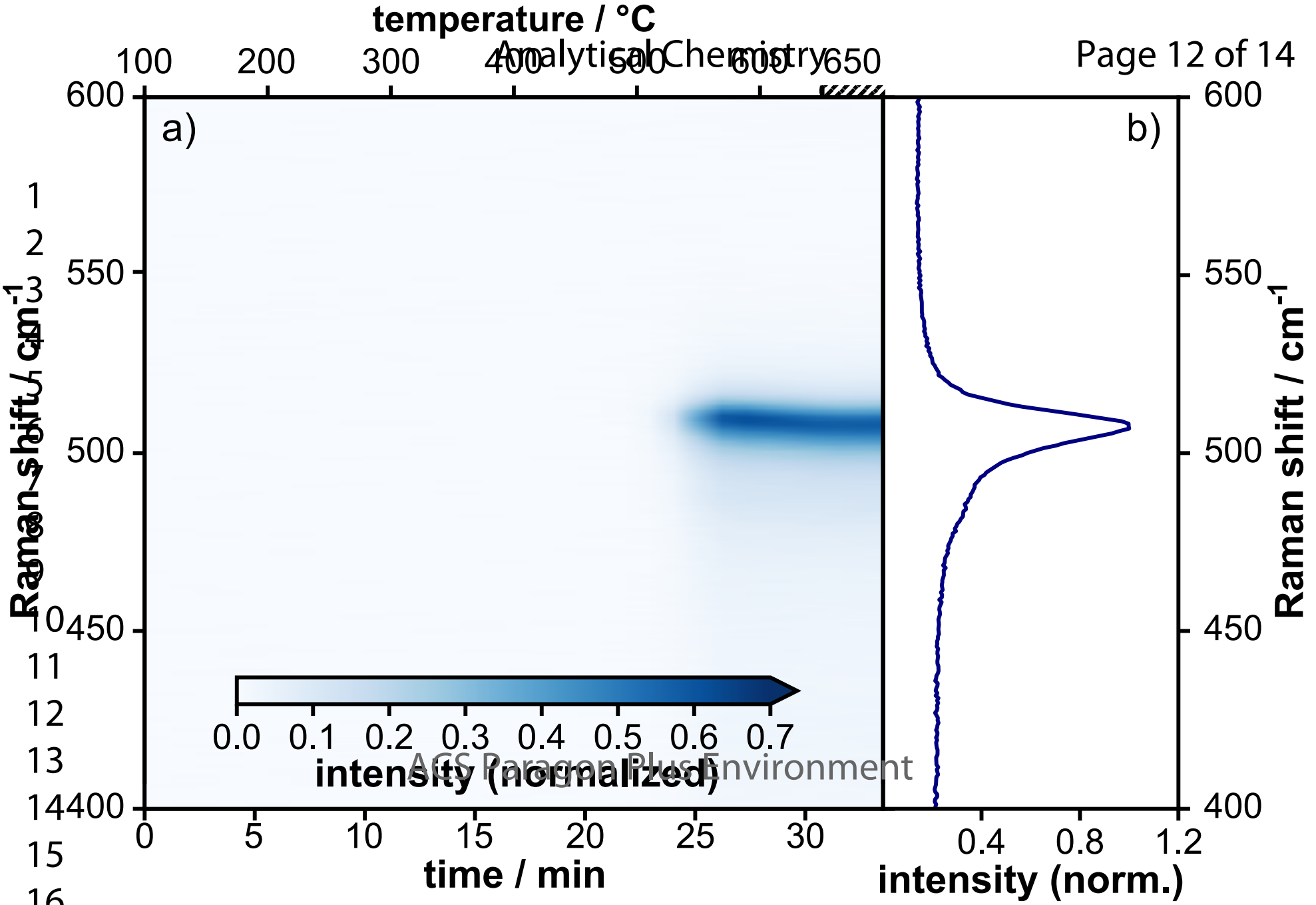

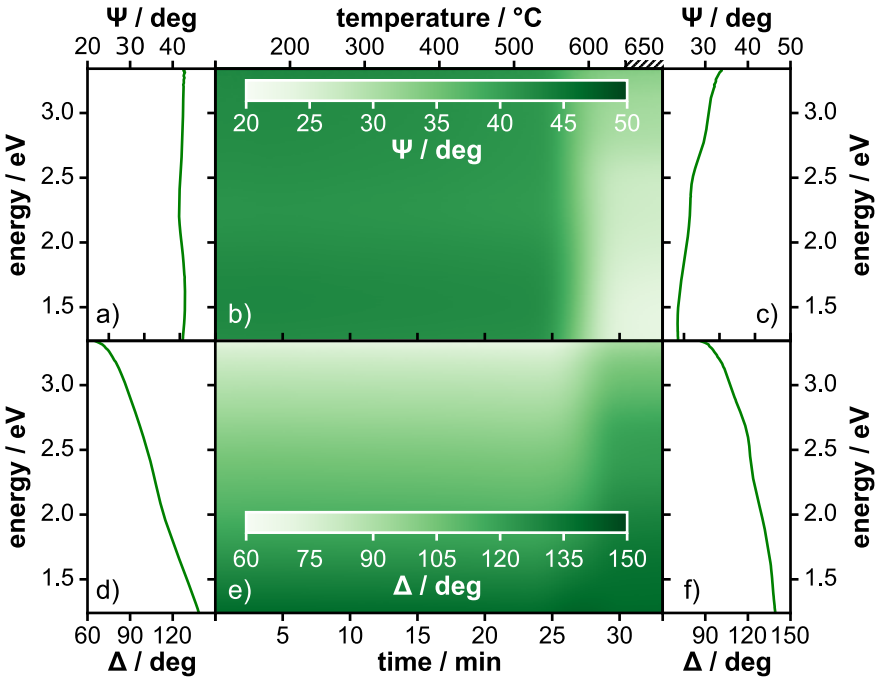
Ψ / deg
temperature / °C
Ψ / deg
20 30 40
200 300 400 500 600 650
30 40 50
20 25 30 35 40 45 50
Ψ / deg
energy / eV
3.0
2.5
2.0
1.5
a)
b)
c)
d)
e)
f)
60 75 90 105 120 135 150
Δ / deg
60 90 120
Δ / deg
5 10 15 20 25 30
time / min
90 120 150
Δ / deg